The response of an equatorial ocean to simple wind stress patterns: I. Model formulation and analytic results

by Mark A. Cane[1]

ABSTRACT

A simple model is developed to study the wind-driven equatorial ocean circulation. It is a time dependent, primitive equation, beta plane model that is two-dimensional in the horizontal. The vertical structure consists of two layers above the thermocline with the same constant density. The ocean below the thermocline is taken to be of a higher constant density and to be approximately at rest. The surface layer is of constant depth and is acted upon directly by the wind. The depth of the lower active layer is dynamically determined. This is the simplest vertical structure which allows a steady state undercurrent.

The linear dynamics of the model are investigated analytically. The circulation evolves on two timescales: a frictional component is established in 0 (20 days) while the pressure gradients and interior flow have a longer, highly variable setup time. The steady transport consists of a Sverdrup part and a frictionally driven part in the vicinity of the equator. When forced with a uniform easterly wind, the flow at the equator in the lower layer is in the same direction as the undercurrent (eastward). However, the vertically integrated transport is westward. This differs from observations and suggests that inertial effects must be included to properly simulate the undercurrent.

In a companion paper (Cane, 1979) both the linear and nonlinear dynamics of the model are investigated by numerical methods.

1. Introduction

Since the vertical component of the Coriolis force vanishes at the equator, the geostrophic balances which dominate the dynamics of the extra-equatorial oceans must break down. The most striking physical manifestation of this singularity is the Equatorial Undercurrent, a narrow (half width of 1°), fast (speeds up to 170 cm/sec), eastward flowing subsurface current in the thermocline of all the world's oceans. (While it is a permanent feature in the Atlantic and Pacific at most longitudes, it has been observed only intermittently in the Indian Ocean, Knox, 1976.) Many of the characteristics of the undercurrent are highly variable: e.g., the downstream velocities and transports may vary by a factor of two or more at different longitudes or at different times. Available observational data allow many of these variations to be

1. NASA/Goddard Space Flight Center, Laboratory for Atmospheric Sciences, Greenbelt, Maryland, 20771, U.S.A.

related systematically to variations in the winds over the equatorial ocean. However, the evidence is, in general, too spotty to allow such correlations to be conclusive. (Philander (1973b) presents a thorough review of the measurements of the undercurrent made up to 1973.)

A second important consequence of the vanishing of the Coriolis term is that equatorial motions have time scales which are very much shorter than those of midlatitude motions: the baroclinic time scale is weeks at the equator, as against years at midlatitudes. The most impressive instance of this short time scale is the reversal in direction of the Somali Current within a month of the onset of the Southwest Monsoon (e.g., Leetmaa, 1973).

Because of the rapidity of the response to atmospheric forcings, equatorial oceans are rewarding areas for the study of motions with time scales of a month or longer. Until quite recently such motions received little theoretical attention. Much of the work in this area has followed Lighthill (1969) in focusing on the set-up of the Somali Current in response to the onset of the Southwest Monsoon. The time dependent behavior of the undercurrent itself has received far less attention. Gill (1975) applied a Lighthill-like model to the undercurrent in the western Pacific. He associated the undercurrent with the second baroclinic mode Kelvin wave which propagates in from the western boundary. It is not clear how such a model explains the presence of the undercurrent as a more permanent feature. Philander (1976) explained the undercurrent meanders observed during GATE (Düing *et al.*, 1975) as the result of a shear instability of the surface currents.

In contrast to the situation for time varying equatorial currents, numerous theoretical models for the steady state undercurrent appear in the literature. These have been reviewed by both Gill (1975) and Philander (1973b). For this reason we shall forego a detailed review here; rather, we shall discuss them only to the extent needed to establish a theoretical context for the present work. On the basis of his observations in the Pacific, Knauss (1966) estimated that the only negligible terms in the momentum equation were those giving the time rate of change of momentum and the horizontal component of the Coriolis force due to vertical motion. (He did not consider horizontal eddy diffusion processes.) The upshot is that a great variety of processes are available to be used as explanations for the undercurrent. Since there is a certain amount of freedom in the choice of eddy coefficients, all of these can be expected to give agreement with at least some of the observed scales. In what follows, we seek to isolate those processes which are most significant.

We shall immediately restrict ourselves to those models which idealize the thermocline as a discontinuity between a shallow upper homogeneous layer and a deeper lower homogeneous layer of greater density. The lower layer is assumed to be so deep that its horizontal pressure forces and velocities vanish. Models with thermohaline components (Robinson, 1960; Philander, 1971, 1973a) are required to explain certain effects at depth; for example, the double celled structure often observed

in the Pacific (see Philander, 1973b). Homogeneous models appear to be sufficient for explaining observed features above the thermocline.

The most basic physical notion about the undercurrent is the idea of flow down a pressure gradient (Charney, 1960). The prevailing easterly winds pile up water at the western side of the ocean basin, thus establishing an eastward pressure gradient. Stommel (1960) exploited this idea to obtain an eastward flowing subsurface current in a linear model with vertical friction. He assumed free slip boundary condition at the bottom and that the vertically integrated transport vanishes at the equator. In a similar model without the latter two assumptions, Charney (1960) and Philander (1971) found that the current at the equator did not reverse with depth. In any case, one would wish any theory to account for the substantial eastward transports observed at the equator. In the linear theory of Gill (1971), the pressure gradient force is balanced by the horizontal mixing of momentum. By using an unrealistically large value for the coefficient of horizontal eddy viscosity (10^8 cm^2 sec^{-1}), Gill obtains the observed latitudinal scale for the undercurrent, but the transport is too low by a factor of at least four.

Nonlinear theories have ignored the downstream inertial terms. The (suspect) assumption is made that the zonal and meridional velocities have the same scale. Then, since the meridional length scale (an equatorial boundary layer scale) is so much shorter than the zonal one (the length of the basin), it follows that in the momentum equation the downstream inertial term is negligible relative to the cross-stream inertial term. Attention is then directed to the meridional circulation. For an easterly wind, the Ekman drift in the surface layers will be poleward. Continuity then requires a compensatory equatorward mass flux at depth, producing an upwelling region at the equator to complete the fluid circuit. Fofonoff and Montgomery (1955) considered the subsurface flow in the light of the barotropic vorticity equation. If it is assumed that a parcel approximately conserves the vertical component of its absolute vorticity, it must change its relative vorticity to make up for the loss of planetary vorticity as it moves equatorward. This results in an eastward flow at the equator. It may also be shown that the meridional circulation near the equator enhances the eastward transport at the equator regardless of whether the wind is easterly or westerly. (See Robinson (1966) for an analytic demonstration; Gill (1975) gives a more physical argument.)

The models of Charney (1960), Charney and Spiegel (1971), Robinson (1966), and McKee (1973) all incorporate the nonlinear effects due to the circulation in the meridional plane. The first three include momentum mixing in only the vertical direction. McKee's model is an extension of Gill's (1971) model into the nonlinear regime; horizontal eddy viscosity is the important frictional force here. A more realistic value for the zonal velocity is obtained compared to the linear model, but an unreasonably large value for the eddy coefficient is again used (10^8 cm^2 sec^{-1}) to obtain the observed undercurrent width. The models of Charney (1960) and

Charney and Spiegel (1971) (the first calculates the flow only at the equator by assuming it is an axis of symmetry; the second paper extends the first model to a meridional plane) give the observed undercurrent velocity and width using a value for the vertical eddy viscosity coefficient (15 cm^2 sec^{-1}) in agreement with existing observational evidence (See Sec. 2). This model also gives good agreement with the observed vertical profile of the undercurrent. Vertical viscosity must be of some importance at depth in order to obtain a nonconstant profile below the boundary layer. Most importantly, a mechanism for the vertical exchange of momentum is needed to introduce the wind stress into the water. There is no similar logical necessity for introducing a significant amount of horizontal mixing. Further, there is no evidence that modeling such mixing gives better agreement with observations.

Previous work thus shows that it is necessary to consider vertical eddy viscosity and inertial effects but not lateral eddy viscosity in order to model the undercurrent effectively. As noted above, all of these models neglect any variation in the zonal direction (except that the zonal pressure gradient is taken as constant). This makes it impossible to ask a number of interesting questions; for example, one cannot investigate the undercurrent meanders observed during GATE. More generally, the issue of the relation of the undercurrent to the entire equatorial current system cannot be explored without considering the whole ocean basin. Since there is a substantial eastward transport at the equator, there must be compensating westward flow elsewhere in the ocean basin. Further, many time varying effects are inseparable from zonal variations. For example, the length of time it takes for the sea surface to set up from rest in response to a wind stress is determined by the speed of waves which propagate in from the boundaries of the basin.

In order to investigate questions of this sort, our model will be time dependent and two dimensional in the horizontal. Since the phenomena of interest are confined to an area near the equator, the basin need not have a great latitudinal extent; 15S to 15N has proven to be sufficient. The model equations are solved numerically because it is imperative that they be fully nonlinear.

In order to make it practical to perform many numerical integrations, the vertical structure is drastically simplified. It consists of two layers above the thermocline with the same constant density. The ocean below the thermocline is taken to be of a higher constant density and to be approximately at rest. The upper of the two active layers is a constant depth surface layer which is acted upon directly by the wind stress. The lower active layer is not directly affected by the wind. Its depth is variable, with the variations being dynamically determined. The two layers communicate via the vertical velocity at their interface as well as being frictionally coupled. *This is the simplest vertical structure that allows a steady undercurrent.*

Of course, this simplification prevents the simulation of the detailed vertical structure of the undercurrent. It is not our intention to do such numerical simulations. Previous work (especially Charney and Spiegel, 1971) provides a bridge for relating

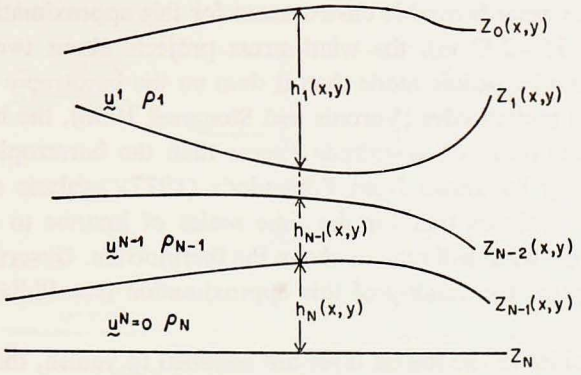

Figure 1. Multi-layer model.

the results of our simple model to the real world. Our philosophy is to treat the numerical experiments in the manner of laboratory experiments: we do not seek to simulate the real world; we seek merely to preserve enough analogy to the real world for the results to give insight into natural phenomena.

There are a large number of phenomena which may be investigated with such a model. In the present study we impose very simple wind stress patterns and study the evolution from a state of rest and eventual steady state configuration of the model ocean. In this paper the model is formulated and its linearized dynamics are explored by analytic means. Numerical results are discussed in the sequel to this work, Cane (1979), henceforth referred to as II. The analytic results are of interest in their own right in addition to being an invaluable aid in the interpretation of the numerical experiments. The vertical structure of the model is novel and these results help to clarify the relationship of the model variables to more familiar oceanographic models. They provide a descriptive vocabulary, a check on the numerical results, and a contrast that highlights the nonlinear effects.

2. Formulation of the physical model

The equations and parameters governing the model are discussed in this section. We begin by considering the familiar layered model in order to see why it is inappropriate for modeling the steady undercurrent. The equations for the model structure employed here are then derived, after which the choice of parameter values is discussed.

a. Layered model. Since we are concerned with inertial and viscous dynamics of a wind-driven ocean, thermohaline effects will be ignored. We divide the ocean vertically into stable material layers of constant density which are assumed to be nonmixing (Fig. 1). We now identify the bottom layer with the water mass below the thermocline and regard it as being sufficiently deep so that its velocity vanishes.

Equatorial regions are a favorable environment for this approximation: the thermocline is shallow (150-200 m), the wind stress projects about twenty times more strongly on the first baroclinic mode than it does on the barotropic mode (Lighthill, 1969), and unlike midlatitudes (Veronis and Stommel, 1956), the baroclinic signals are only about one order of magnitude slower than the barotropic. Further theoretical support may be drawn from Philander's (1977) analysis of vertical wave propagation, which shows that for the time scales of interest to us, most of the energy put in by the wind will remain above the thermocline. Observational evidence also tends to support the validity of this approximation (see Philander, 1973b for a summary).

Since the velocities in the lowest layer are assumed to vanish, the pressure gradient must vanish there as well. This leaves us with the familiar "reduced gravity" model; for a single active layer the equations governing the *average* horizontal current and the layer depth h_1 are

$$\frac{\partial}{\partial t}\,\mathbf{u}^1 + (\mathbf{u}^1 \cdot \nabla)\,\mathbf{u}^1 + f\,\mathbf{k} \times \mathbf{u}^1 = -g'\,\nabla h_1 + (\boldsymbol{\tau}_0 - \boldsymbol{\tau}_1)\,h_1^{-1} + \nu_H\,\nabla^2\,\mathbf{u}^1 \tag{2.1}$$

$$\frac{\partial}{\partial t}\,h_1 + \nabla \cdot (h_1\,\mathbf{u}^1) = 0. \tag{2.2}$$

Where the reduced gravity $g' = g\,(\rho_2 - \rho_1)/\rho_2$, $\boldsymbol{\tau}_0$ is the wind stress, $\boldsymbol{\tau}_1$ the interfacial stress between the two layers and $\nu_H \nabla^2 \mathbf{u}^1$ is the horizontal eddy stress.[2] The components of the Coriolis force due to vertical motions and departures from hydrostatic balance are neglected; this may be justified a posteriori.

The wind stress appears as a body force in (2.1). This is a commonly used modeling procedure in oceanography that can be rigorously justified for many purposes (e.g. Charney, 1955). However for some purposes, such as modeling the undercurrent, a difficulty is created by introducing the wind stress as a body force averaged over the uppermost layer.

For a constant easterly wind stress (of magnitude τ per unit mass) the steady state solution to (2.1), (2.2) is

$$\mathbf{u}^1 = 0;\ h_1^2 = h_1^2\,(x{=}0) + x\,\tau/g'. \tag{2.3}$$

The zonal pressure gradient is balanced by the wind stress at all depths. In reality this pressure gradient is sufficient to drive the equatorial undercurrent because the fluid at depth feels the pressure force but not the wind stress (Charney, 1960; Gill, 1971). Obviously the layered model misses this effect.

2. The usual finite difference assumption about quadratic terms has been made, that

$$h_1^{-1} \int_{z_1}^{z_0} (\mathbf{u} \cdot \nabla)\,\mathbf{u} \approx \mathbf{u}^1 \cdot \nabla\,\mathbf{u}^1.$$

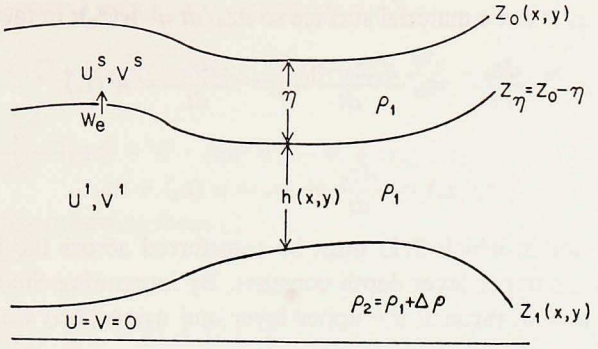

Figure 2. Model with two active layers.

Similar no-motion solutions can easily be found for a multilayer model whether or not the bottom layer is constrained to be motionless: the layer depths may always adjust to reduce the pressure gradient to zero in each subsurface layer. For example, with some dissipation in the system a two layer model with its lower layer not constrained to be motionless will still evolve to such a motionless steady state. (This model does permit a *transient* undercurrent.)

It should be emphasized that such models are not wrong in some simple sense. In fact, the profile of the thermocline depth specified by (2.3) is very close to what is observed at the equator (cf. Gill, 1975, Fig. 3). The difficulty is that the feature of interest is missed by the layered models because they consider only the depth averaged currents within each layer. A correct treatment of the wind stress would introduce it as a boundary condition e.g. $\nu_v u_z = \tau_{\text{wind}}$ at the surface, so the velocity cannot vanish at all depths. The vertically *averaged* velocities may vanish. For the example discussed above, this could come about at the equator if the surface flow driven westward by the wind stress were just compensated by the flow at depth driven eastward by the pressure force. In reality, inertial effects act nonuniformly with depth to give a net eastward transport at the equator. This is precisely the mechanism for generating an undercurrent referred to in Sec. 1.

b. Model equations. To capture this essential mechanism we modify the model with a single active layer by dividing this layer into two parts: a surface layer of *constant* depth η and a lower layer of variable depth h (Fig. 2). There is *no density difference* between these two layers and transfer of mass and momentum between the two is permitted. The wind stress is felt directly only by the surface layer; in this sense this layer plays the role of the ocean mixed layer.

Denote the average of a quantity q over the upper active layer by q^s and over the lower layer by q^1; i.e.

$$q^s = \eta^{-1} \int_{z_\eta}^{z_0} q\, dz;\ q^1 = h^{-1} \int_{z_1}^{z_\eta} q\, dz\,. \tag{2.4}$$

The surface $z = z_\eta$ is not a material surface so $dz_\eta/dt \neq w(z_\eta)$; in fact

$$\frac{dz_\eta}{dt} = \frac{d\,(z_0 - \eta)}{dt} = \frac{dz_0}{dt} = w\,(z_0) \tag{2.5}$$

and

$$w\,(z_\eta) = \frac{dz_\eta}{dt} + w_e = w\,(z_0) + w_e \tag{2.6}$$

where w_e is the rate at which fluid must be transferred across the interface $z = z_\eta$ in order to keep the upper layer depth constant. By integrating the continuity equation, $w_z + \nabla \cdot \mathbf{u} = 0$, through the upper layer and using (2.6) we may obtain the relation

$$w_e = w\,(z_\eta) - w\,(z_0) =$$

$$\int_{z_\eta}^{z_0} \nabla \cdot \mathbf{u}\, dz = \nabla \cdot \int_{z_\eta}^{z_0} \mathbf{u}\, dz - \{\mathbf{u}\,(z_0) \cdot \nabla z_0 - u\,(z_\eta) \cdot \nabla z_\eta\}\,.$$

Since

$$\{\mathbf{u}\,(z_0) \cdot \nabla z_0 - u\,(z_\eta) \cdot \nabla z_\eta\} =$$

$$\left\{\frac{dz_0}{dt} - \frac{\partial z_0}{\partial t}\right\} - \left\{\frac{dz_\eta}{dt} - \frac{\partial z_\eta}{\partial t}\right\} = \frac{d}{dt}\{z_\eta - z_0\} - \frac{\partial}{\partial t}\{z_\eta - z_0\} = 0$$

it follows that

$$w_e = \nabla \cdot (\eta \mathbf{u}^s) = \eta \nabla \cdot \mathbf{u}^s\,, \tag{2.7a}$$

so that entrainment balances the divergence in the surface layer. A similar manipulation on the continuity equation integrated from z_0 to z_1 yields

$$\frac{\partial h}{\partial t} = -\nabla \cdot (h\mathbf{u}^1) - w_e\,; \tag{2.7b}$$

the depth of the lower layer is changed either by divergence of fluid within the layer or by exchanges with the layer above.

To derive the momentum equations for the two layers we begin with the momentum equation in the form

$$\mathbf{R} = \frac{\partial \mathbf{u}}{\partial t} + \mathbf{u} \cdot \nabla \mathbf{u} + w \frac{\partial \mathbf{u}}{\partial z} = \frac{\partial}{\partial t}\mathbf{u} + \nabla \cdot (\mathbf{uu}) + \frac{\partial}{\partial_z}(w\mathbf{u})$$

with $\mathbf{R}$ standing for all the other terms in the equation. Integrating over the upper layer and using Leibnitz's rule

$$\int_{z_\eta}^{z_0} \mathbf{R}\, dz = \left\{\frac{\partial}{\partial t}\int_{z_\eta}^{z_0} \mathbf{u}\, dz - \left[\mathbf{u}\,(z_0)\frac{\partial z_0}{\partial t} - \mathbf{u}\,(z_\eta)\frac{\partial z_\eta}{\partial t}\right]\right\}$$

$$+ \left\{\nabla \cdot \int_{z_\eta}^{z_0} \mathbf{u}\,\mathbf{u}\, dz - [\mathbf{u}(z_0)\,(\mathbf{u}(z_0) \cdot \nabla z_0) - \mathbf{u}(z_\eta)\,(\mathbf{u}(z_\eta) \cdot \nabla z_\eta)]\right\}$$

$$+ w(z_0)\,\mathbf{u}(z_0) - w(z_\eta)\,\mathbf{u}(z_\eta)$$

$$= \frac{\partial}{\partial t}(\eta \mathbf{u}^s) + \nabla \cdot (\eta \mathbf{u}^s \mathbf{u}^s) - \mathbf{u}(z_0)\frac{dz_0}{dt} + \mathbf{u}(z_\eta)\frac{dz_\eta}{dt} + w(z_0)\mathbf{u}(z_0) - w(z_\eta)\,\mathbf{u}(z_\eta);$$

$$\int_{z_\eta}^{z_0} \mathbf{R}\,dz = \frac{\partial}{\partial t}(\eta \mathbf{u}^s) + \nabla \cdot (\eta \mathbf{u}^s\,\mathbf{u}^s) - w_e\,\mathbf{u}(z_\eta) \tag{2.8a}$$

with the last equality following from (2.6).
In the lower layer

$$\int_{z_1}^{z_\eta} \mathbf{R}\,dz = \frac{\partial}{\partial t}\int_{z_1}^{z_\eta} \mathbf{u}\,dz + \nabla \cdot \int_{z_1}^{z_\eta} \mathbf{u}\,\mathbf{u}\,dz - u(z_\eta)\frac{dz_\eta}{dt} + u(z_1)\frac{dz_1}{dt}$$
$$+ w(z_\eta)\,u(z_\eta) - w(z_1)\,\mathbf{u}(z_1),$$

$$\int_{z_1}^{z_\eta} \mathbf{R}\,dt = \frac{\partial}{\partial t}(h\mathbf{u}^1) + \nabla \cdot (h\mathbf{u}^1\mathbf{u}^1) + w_e\,\mathbf{u}(z_\eta) \tag{2.8b}$$

To close the set of equations (2.7), (2.8) $u(z_\eta)$ must be expressed in terms of the other variables. Applying the requirement that there be no spurious sources or sinks of energy determines that

$$\mathbf{u}(z_\eta) = \tfrac{1}{2}(\mathbf{u}^s + \mathbf{u}^1) \tag{2.8c}$$

Writing $\mathbf{R}$ explicitly and using (2.7) to go from flux to momentum form gives the final form of the momentum equations.

$$\frac{\partial}{\partial t}\mathbf{u}^s + (\mathbf{u}^s \cdot \nabla)\,\mathbf{u}^s + \frac{w_e}{2\eta}(\mathbf{u}^s - \mathbf{u}^1) + f\,\mathbf{k} \times \mathbf{u}^s$$
$$= -g'\nabla h + \frac{\tau_0}{\eta} - \frac{K}{\eta}(\mathbf{u}^s - \mathbf{u}^1) + \nu_H \nabla^2 \mathbf{u}^s, \tag{2.9a}$$

$$\frac{\partial}{\partial t}\mathbf{u}^1 + (\mathbf{u}^1 \cdot \nabla)\,\mathbf{u}^1 + \frac{w_e}{2h}(\mathbf{u}^s - \mathbf{u}^1) + f\,\mathbf{k} \times \mathbf{u}^1$$
$$= -g'\nabla h - \frac{K_B}{h}\mathbf{u}^1 + \frac{K}{h}(\mathbf{u}^s - \mathbf{u}^1) + \nu_H \nabla^2 \mathbf{u}^1, \tag{2.9b}$$

The stresses at the interfaces, $\boldsymbol{\tau}(z_\eta)$, and $\boldsymbol{\tau}(z_1)$ have been modeled in a simple linear fashion:

$$\boldsymbol{\tau}(z_\eta) = K(\mathbf{u}^s - \mathbf{u}^1);\ \boldsymbol{\tau}(z_1) = K_B\,\mathbf{u}^1. \tag{2.10}$$

In terms of the vertical eddy viscosity ν_v $\boldsymbol{\tau} = \nu_v\,\partial\mathbf{u}/\partial z$ so we may argue heuristically that

$$K = K_B = \nu_v/H_\bullet \tag{2.11}$$

with $H_\bullet$ a characteristic vertical distance between fluid elements in the active layers.

Table 1. Standard Values of Model Parameters.

Parameter	Value	Remarks
τ	.465 dyn cm^{-2}/(gm cm^{-3})	Wind stress per unit mass
g'	.1724 msec^{-2}	"reduced gravity" $g' = g\,(\rho_2-\rho_1)/\rho_2$ for $(\rho_2-\rho_1)/\rho_2 = 1.86 \times 10^{-2}$
ν_H	5.86×10^5 cm^2 sec^{-1}	coefficient of horizontal viscosity
ν_v	15 cm^2 sec^{-1}	coefficient of vertical viscosity
K	1.5×10^{-3} msec^{-1}	interfacial friction parameter; $K = \nu_v/H^*$ for $H^* = 100$ m
K_B	1.5×10^{-3} msec^{-1}	bottom friction parameter; $K_B = K$
X_B	28.6° (3184 km)	zonal extent of the basin
θ_T	15°	basin walls are at 15N and 15 S
θ_B	−15°	
η	25 m	depth of upper layer
$\bar{H}_1$	175 m	mean value of the lower layer depth h
β	2.2×10^{-11}m^{-1}sec^{-1}	$\beta = (df/dy)_{y=0} = 2\Omega/R$ where $\Omega = 2\pi$ day^{-1} and R is the radius of the earth

Finally, at all lateral boundaries we impose no-slip boundary conditions

$$\mathbf{u}^3 = \mathbf{u}^1 = 0\,. \tag{2.12}$$

c. Choice of parameter values. The values for the model parameters given in Table 1 are by and large typical values for equatorial oceans. Placing the zonal coasts at ±15° makes them sufficiently far from the equator so that their presence has negligible influence on the dynamics in the vicinity of the equator (8S to 8N). The possibility of separating the effects of zonal walls from the equatorial dynamics depends on these dynamics being locally determined; i.e., "trapped" to the equator. That this is the case is borne out by our subsequent analytic investigations (also see Cane and Sarachik, 1976, 1977); it is also evident from the flow field pictures obtained from the numerical calculations (see II). Additional shorter numerical experiments with the zonal walls 20° from the equator differed little near the equator from those with the walls at 15°. The zonal width of the basin is smaller than that of the world's oceans, but is large enough to have a broad interior region where the dynamics may be clearly separated from the dynamics of the meridional boundary layers. The model ocean is taken to be on an equatorial beta plane (e.g. Veronis, 1963a, b) with the Coriolis parameter $f = \beta y$.

Vertical eddy diffusion is to be the principal dissipative mechanism in the model. We choose H_* to be 100 meters (one half of the depth of the active layers) and use (2.11) to relate the K's to the vertical eddy viscosity coefficient ν_v. Knauss (1966) calculated a value of 5 cm^2 sec^{-1} by fitting a parabola to the velocity profile of the undercurrent observed in the Pacific. Williams and Gibson (1974) applied universal similarity and local isotropy assumptions to measurements of small scale temperature fluctuation at 150W and a depth of 100 m. They found values of ν_v of 25 cm

sec^{-1} at the equator and 12 cm sec^{-1} at 1N. Charney (1960) and Charney and Spiegel (1971) found that their models best fit the observed undercurrent for a value of the eddy viscosity in the range 14-17 $\text{cm}^2\ \text{sec}^{-1}$. In the light of this evidence, we use 15 $\text{cm}^2\ \text{sec}^{-1}$ as a standard value for ν_v, feeling some confidence in (at least) the order of magnitude of the choice. The horizontal eddy viscosity is taken small enough to have negligible effect on the interior dynamics. A nonzero value is needed if the boundary conditions (2.12) are to be satisfied.

The presence of the surface layer introduces another parameter, the layer depth η. The numerical value we attach to η will determine how the vertically integrated transport is divided between the two active layers. For example, if $\eta = 25$ m and $\bar{H}$, the total depth of the layer, is 200 m, then u^s is the average zonal velocity in the top 25 m and u^1 is the average zonal velocity in the next 175 m. Their depth-weighted sum $25\ u^s + 175\ u^1$ is the zonal transport. The choice of the surface layer depth has two effects on the model physics, as may be seen by considering its effect on the transport equations. First, the bottom drag is proportional to the lower layer velocity, whose value will depend on the value of η. This is true even in a linear model (cf. Sec. 3). The second effect is nonlinear, and comes about because we make the modelling assumption that the velocities are independent of depth within each layer. This means that the way we choose to divide up the average velocity affects the size of the nonlinear terms.

Because the choice of the surface layer depth does affect the model physics, we seek a physical basis for determining its value. Unfortunately, the available observational evidence from the world's oceans is not sufficient to help us choose this parameter. We make the choice on theoretical grounds. Consider a shallow homogeneous ocean driven by an imposed wind stress. The ocean is specified to be shallow so that the horizontal component of the Coriolis force may be ignored everywhere. Extra-equatorially, the wind stress is felt in an Ekman layer of depth $D_E = \{2\nu_v/f\}^{\frac{1}{2}}$. Below this boundary layer (and away from the bottom) the dynamics are inviscid and it is transmitted via the boundary layer pumping of the Ekman layer. (See, for example, Charney, 1955; Pedlosky, 1968; or Robinson, 1970 for a detailed account.) As the equator is approached, the Ekman depth D_E increases, becoming infinite at the equator in the absence of additional dynamical balances. We are, however, interested in modelling a parameter range when the wind stress is sufficiently strong and the value of the vertical viscosity sufficiently small so that inertial effects become important in the vicinity of the equator. A measure of these effects in the boundary layer is the Rossby number R_0 based on the boundary layer velocity. For a wind stress per unit mass of magnitude τ the velocity scale in the Ekman layer is given by $U = \tau/(D_E f)$. Then $R_0 = U/(fy) = \tau\ [2\nu_v\beta^3 y^5]^{-\frac{1}{2}}$ so that

$$y = R_0^{-2/5}\ [\tau^2/(2\nu_v\beta^3)]^{1/5} \tag{2.13}$$

The inertial terms will enter into the boundary layer momentum balance (along

with the Coriolis and vertical friction terms) when $R_0 = 0(1)$. As the equator is approached, R_0 increases so that equatorward of some latitude Y_C the inertial effects will prevent the boundary layer from deepening any further. In fact, if the velocities increase toward the equator, we may expect that the boundary layer will get shallower. If we assume that the boundary layer stops deepening when $R_0 = .5$ and use the values in Table 1 (i.e, $\tau = .5$ cm^2 sec^{-2}, $\nu_v = 15$ cm^2 sec^{-1}), we obtain $Y_C = 2°$. The Ekman depth D_E is approximately 25 m at this latitude. [Neither of these is very sensitive to the precise value of R_0 for $R_0 = 0(1)$.] These values agree well with Charney and Spiegel's (1971) calculation for the same parameter values (see their Fig. 1). On the basis of this argument we choose the value $\eta = 25$ m, so that our surface layer will contain the boundary layer to be expected from a continuous model.

3. Formulation of the mathematical problem

To facilitate analytic treatment of Eqs. (2.7), (2.9) we scale the variables as follows:

$$(x,y) = L\,(x',y') \qquad (\mathbf{u}^s,\mathbf{u}^1) = u\,(\mathbf{u}^{s\prime},\mathbf{u}^{1\prime})$$
$$\eta = \bar{H}\,\alpha \qquad w_e = [u\bar{H}/L]\,w_e'$$
$$h = \bar{H}_1 + [U\beta L^2/g']\,h' \qquad \boldsymbol{\tau} = \tau_0\,\boldsymbol{\tau}'$$
$$t = Tt'$$

Here $\bar{H}_1$ is the mean depth of the lower active layer and $\bar{H} = \bar{H}_1 + \eta$.

The velocity scale is related to the wind stress magnitude by $U = \tau_0\,(\bar{H}\beta L)^{-1}$. We take the length and time scales as the baroclinic equatorial ones (e.g., Matsuno, 1966; Blandford, 1966): $L = (c/\beta)^{\frac{1}{2}}$ and $T = (c\beta)^{\frac{1}{2}} = (\beta L)^{-1}$, where $c = (g'\bar{H})^{\frac{1}{2}}$. These length and time scales are internal scales, picked out by the dynamics of the fluid motions. We assume that the wind stress is a smooth function at these scales and that the dimensions of the basin are large compared with L. (For the values in Table 1, $L = 296$ km, $T = 42.6$ hours and $c = 1.92$ m sec^{-1}.)

Dropping the primes and denoting differentiation with subscripts the scaled equations are:

$$\mathbf{u}_t^s + \epsilon\,\{(\mathbf{u}^s \cdot \nabla)\,\mathbf{u}^s + \frac{w_e}{2\alpha}\,(\mathbf{u}^s - \mathbf{u}^1)\} + y\,\mathbf{k} \times \mathbf{u}^s$$
$$= -\nabla h + \boldsymbol{\tau}/\alpha + A\,\nabla^2\,\mathbf{u}^s - \gamma_I\,(\mathbf{u}^s - \mathbf{u}^1)/\alpha\,, \tag{3.1a}$$

$$\mathbf{u}_t^1 + \epsilon\,\{(\mathbf{u}^1 \cdot \nabla)\,\mathbf{u}^1 + \frac{w_e\,(\mathbf{u}^s - \mathbf{u}^1)}{2\,(1-\alpha+\epsilon h)} + y\,\mathbf{k} \times \mathbf{u}^1$$
$$= -\nabla h + A\,\nabla^2\,\mathbf{u}^1 + \frac{\gamma_I\,(\mathbf{u}^s - \mathbf{u}^1)}{1-\alpha+\epsilon h} - \frac{\gamma}{1-\alpha+\epsilon h}\,\mathbf{u}^1\,, \tag{3.1b}$$

$$w_e = \alpha\,\nabla \cdot \mathbf{u}^s\,, \tag{3.1c}$$

$$h_t + (1-\alpha) \nabla \cdot \mathbf{u}^1 + \alpha \nabla \cdot \mathbf{u}^s + \epsilon \nabla \cdot (h\mathbf{u}^1) = 0 . \tag{3.1d}$$

where the following nondimensional numbers have been introduced:

Rossby number	$\epsilon = U/(\beta L^2)$;
Horizontal Ekman number	$A = \nu_H/(\beta L^3)$;
Interfacial Ekman number	$\gamma_I = K/(\beta L \bar{H})$;
Bottom Ekman number	$\gamma = K_B/(\beta L \bar{H})$;
Nondimensional boundary layer depth	$\alpha = \eta/\bar{H}$.

(3.2)

The last three of these numbers, while logically independent as the model is formulated, are all related to vertical friction and so may be related to one another. First, with $K = K_B$ we have $\gamma_I = \gamma$. From the arguments of Sec. 2c we expect η to be on the order of the Ekman depth, η_E, at the edge of the equatorial boundary layer $y = L$ (since $L \approx Y_c$). Now

$$\eta_E = (2\nu_v/f)^{\frac{1}{2}}{}_{y=L} = [2KH^*/(\beta L)]^{\frac{1}{2}} = \gamma^{\frac{1}{2}} [2H_*/\bar{H}]^{\frac{1}{2}}$$

where H^* is a characteristic layer depth. As before we take $H^* = \bar{H}/2$, so $\alpha = 0\,(\eta_E/\bar{H}) = 0\,(\gamma^{\frac{1}{2}})$.

We are interested in parameter ranges for which vertical friction is more important than horizontal friction: $A << \gamma, \gamma_I$. We also assume that $\gamma^{\frac{1}{2}} < 0(1)$. (For the values of the parameters given in Table 1, $\alpha = .125$, $A = 10^{-4}$, $\gamma = .011$, $\gamma_I = .1$, and this is the case.[3]) Horizontal friction will be neglected in the interior of the basin, including the equator. As previously mentioned, A must be nonzero to allow the boundary conditions (2.12) to be imposed; if $A = 0$ only the normal component of the transport may be set to zero. Sidewall boundary layers will not be considered further here. Cane, 1975 contains a thorough discussion of boundary conditions and sidewall boundary layers in this model. (See Pedlosky, 1968 or Robinson, 1970 for a discussion of sidewall boundary layers in a continuous, unstratified ocean.)

Since it is the linear dynamics of the model which are to be investigated analytically, we linearize (3.1) by assuming $\epsilon = 0$. It is convenient for this analysis to introduce two new variables:

$$\tilde{\mathbf{u}} \equiv (1-\alpha)\,\mathbf{u}^1 + \alpha\,\mathbf{u}^s; \quad \tilde{\mathbf{u}} \equiv \alpha\,(\mathbf{u}^s - \mathbf{u}^1) \tag{3.3}$$

Then by taking appropriate combiations of (3.1a) and (3.1b) one obtains

$$\tilde{\mathbf{u}}_t + y\,\mathbf{k} \times \tilde{\mathbf{u}} + E\,\tilde{\mathbf{u}} = \boldsymbol{\tau} + A \nabla^2 \tilde{\mathbf{u}} + \frac{\alpha}{1-\alpha} \gamma\,\tilde{\mathbf{u}}\,, \tag{3.4}$$

3. Neglect of A in (3.1a) or (3.4) requires $A<\gamma^{3/2}$; neglect in (3.1b) or (3.5a) requires $A<\gamma^2$, which is only marginally true. The analytic results should be in qualitative agreement with the linear numerical experiments.

$$\tilde{\mathbf{u}}_t + y\,\mathbf{k} \times \tilde{\mathbf{u}} + \nabla h = \boldsymbol{\tau} + A\,\nabla^2 \tilde{\mathbf{u}} - \gamma\,(\tilde{\mathbf{u}} - \tilde{\mathbf{u}}), \tag{3.5a}$$

$$h_t + \nabla \cdot \tilde{\mathbf{u}} = 0, \tag{3.5b}$$

where

$$E = (1-\alpha)^{-1}\,[\alpha^{-1}\,\gamma_I + \alpha\gamma] = 0\,(\gamma^{\frac{1}{2}}). \tag{3.6}$$

In the absence of bottom friction (γ=0) then equations become uncoupled: $\tilde{\mathbf{u}}$ may be determined from (3.4) alone and $\tilde{\mathbf{u}}$,h from (3.5) alone. The quantity $\mathbf{u}$ is the (scaled) vertically integrated mass transport while $\tilde{\mathbf{u}}$ is the frictional layer velocity; extra-equatorially ($y>>E$) $\tilde{\mathbf{u}}$ is just the Ekman layer transport. From (3.3) we may write

$$\mathbf{u}^s = \alpha^{-1}\,\tilde{\mathbf{u}} + \mathbf{u}^1,$$

which says that the surface velocity is given primarily by frictional effects corrected by the interior velocity $\mathbf{u}^1$. Away from the equator $\mathbf{u}^1$ becomes geostrophic. The variables $\tilde{\mathbf{u}}$, $\mathbf{u}^1$ are this two-layer model's analogues of the variables used by Philander (1971) in his analysis of the dynamics of a continuous shallow equatorial ocean.

4. The interior circulation: analytic results

a. Frictional velocity. Eq. (3.4) may be used to obtain $\tilde{\mathbf{u}}$ since the term involving $\tilde{\mathbf{u}}$ is never greater than $O(E^2)$ relative to the retained terms. This equation is first order in time with only a parametric dependence on x and y (with A=0), and so may be solved readily for arbitrary wind stress. It is sufficient to treat only a wind stress that is a step function in time switched on at t=0. In this case

$$\tilde{\mathbf{u}} = [E^2 + y^2]^{-1}\,\{-y\,\mathbf{k} \times \tau + E\,\tau\} \times \{1 - \exp\,[(-E + i\,y)t]\} \tag{4.1}$$

The time scale for the buildup of this component of the current system is clearly E^{-1} — 20 days for the values in Table 1. For short times [$t << O(E^{-1})$] and points sufficiently near the equator [$|y| << O(t^{-1})$] (4.1) simplifies to $\tilde{\mathbf{u}} = t\boldsymbol{\tau}$; i.e. the solution is in the direction of the wind and grows linearly with time. Right at the equator the solution valid for all time is simply $\tilde{\mathbf{u}} = \boldsymbol{\tau}E^{-1}\,\{1-e^{-Et}\}$ so that the $\tilde{\mathbf{u}}$ at the equator is always in the direction of the wind. Its magnitude is limited by the friction between the two layers and approaches $E^{-1}\,|\boldsymbol{\tau}|$ for times long compared with E^{-1}. Away from the equator $\tilde{\mathbf{u}}$ approaches the Ekman wind drift, $-y^{-1}\,\mathbf{k} \times \boldsymbol{\tau}$; it is directed 90° to the right (left) of the wind in the northern (southern) hemisphere.

b. Vertically integrated transport: steady state circulation. The steady state form of the continuity equation (3.5b) allows us to define a mass transport stream function

$$\tilde{\mathbf{u}} = \mathbf{k} \times \nabla \psi. \tag{4.2}$$

satisfying $\psi = 0$ at the boundaries. A vorticity equation may then be derived from (3.5a):

$$\gamma \nabla^2 \psi + \psi_x - \mathbf{k} \cdot \nabla \times \boldsymbol{\tau} = \gamma \, \mathbf{k} \cdot \nabla \times \tilde{\mathbf{u}} \, . \tag{4.3}$$

For the moment we set the right-hand side of (4.3) to zero, reducing it to the Stommel (1948) model for the mass transport stream function. As is well known, this equation admits boundary layers at the zonal boundaries and at the western side of the basin, but not at the eastern side. The appropriate boundary condition for the interior problem is $\psi = 0$ at $x = X_E$, the eastern boundary. Letting $\boldsymbol{\tau} = (\tau^{(x)}, \tau^{(y)})$ the interior solution may be written

$$\begin{aligned} \psi^{(0)} &= -\int_x^{x_E} \mathbf{k} \cdot \nabla \times \boldsymbol{\tau} \, dx \, , \\ h^{(0)} &= -\int_x^{x_E} [y \, \mathbf{k} \cdot \nabla \times \boldsymbol{\tau} + \tau^{(x)}] \, dx + \int^y \tau^{(y)} \, (x = X_E) \, dy \end{aligned} \tag{4.4}$$

If the wind stress curl vanishes everywhere (e.g. for constant $\boldsymbol{\tau}$) then (4.4) says that there is no vertically integrated mass transport; the wind stress is balanced by the pressure gradient force.

In the absence of bottom friction the steady state circulation is completely described by (4.1) and (4.4). However, with γ nonzero the right-hand side of the vorticity equation becomes 0(1) in a region $|y| \leqslant O\,(E)$. Hence there is a region at the equator in which the circulation controlled by the interfacial friction, which itself has no net transport, induces a mean circulation via bottom friction. Letting $\zeta = E^{-2} y$ and writing

$$\psi \, (x,y) = \psi^{(0)} \, (x,y) + \pi \, (x,\zeta) \, , \tag{4.5}$$

where π is the stream function for this frictionally induced circulation, we note that π depends only on the local winds at the equator. Since near the equator

$$\mathbf{k} \cdot \nabla \times \tilde{\mathbf{u}} \approx - E^{-2} \, \mathbf{u}_\zeta{}^{(0)} \equiv E^{-2} \, \{(1 + \zeta^2)^{-1} \, (\zeta \, \tau^{(y)} \, (x,y) + \tau^{(x)} \, (x,y))\}_\zeta$$

[cf. (4.1)], the equation for π derivable from (4.3) is

$$\pi_{\zeta\zeta} + a \pi_x = -\tilde{\mathbf{u}}_\zeta{}^{(0)} \tag{4.6}$$

where $a = \gamma^{-1} E^2 = O(1)$. The solution to (4.6) is derived in Cane (1975) and is depicted (for a=1) in Figures 3 and 4 for uniform easterly and southerly wind stresses.

For a zonal wind stress the net transport at the equator is in the direction of the wind. This is, of course, contrary to what is observed for the undercurrent. It says that we must look to other (i.e. nonlinear) effects to explain the undercurrent. For a meridional wind the transport will be in the direction of the wind drift current in both hemispheres. The fluid circuit will be closed by a weak interior transport directed opposite to the wind and a downwind flow in the western boundary layer.

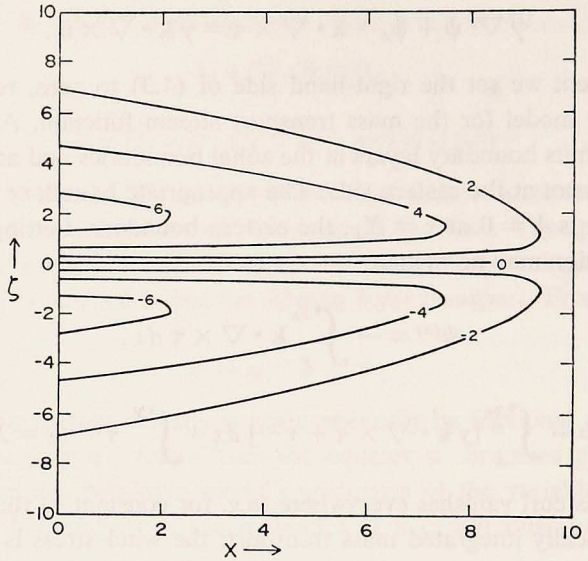

Figure 3. The equatorial boundary layer mass transport stream function $\Pi^{(1)}(x,\zeta)$ of Eq. (3.16) for a uniform easterly wind $\tau^{(x)} = -1$, $\tau^{(y)} = 0$.

For any wind stress pattern the flow will be predominantly zonal [$\bar{v}=O(E\bar{u})$] since flow along the equator is favored. The diffusionlike nature of (4.5) means that the region of frictionally induced transport will broaden from east to west. This description will be compared with the steady state linear numerical results in II.

To summarize, we have found that the steady state interior circulation consists of two parts. The first part, described by (4.1) and (4.3), has a Sverdrup balance everywhere for the transport and essentially a wind drift solution for the boundary layer. The second part, described by (4.6), is important in a region extending about 300 km on either side of the equator. (Note that although $\zeta = 1$ corresponds to only $y =$ 30 km, variables fall off slowly—like ζ^{-1} in some cases.) There is a net transport at the equator in the direction of the zonal wind. Return flow also takes place within this region.

These results may be compared with those of Philander (1971) for a homogeneous ocean continuous in the vertical. For that model, the frictional layer deepens toward the equator and extends throughout the ocean at the equator. The boundary layer in which this happens is embedded in a more diffuse boundary layer in which bottom friction is important. There is a net transport in the direction of the zonal wind in the first of these layers, which is returned in the broader layer. It appears that our modeling assumption, which fixes the boundary layer depth, has the effect of combining these two layers.

c. Vertically integrated transport: time dependent circulation. As with the steady state solution, the time dependent circulation described by (3.5) is best split into

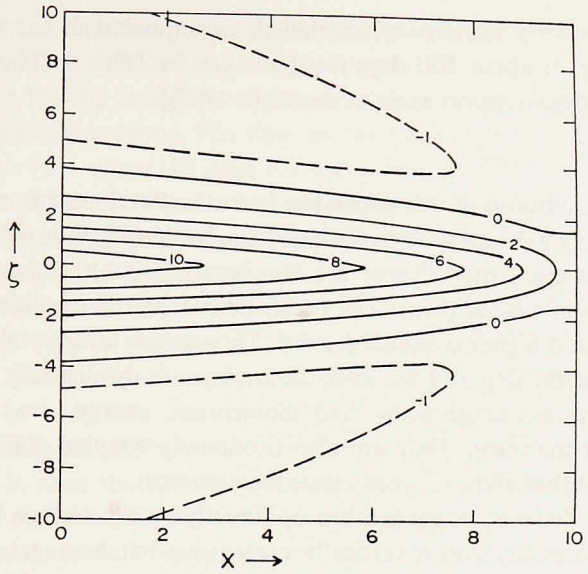

Figure 4. The equatorial boundary layer mass transport stream function $\Pi^{(1)}$ (x,ζ) of Eq. (3.16) for a uniform northerly wind $\tau^{(x)} = 0$, $\tau^{(y)} = 1$.

two parts. By neglecting bottom friction in (3.5a), Eqs. (3.5) become the inviscid shallow water equations on an equatorial beta plane, which may be solved by the methods of Cane and Sarachik (1976, 1977) for all cases of interest here. We will use their results in subsequent descriptions of linear numeral calculations, but for now we only state some of the implications of their work for the spin-up of the present model.

Adjustment toward a final steady state proceeds from east to west and is accomplished by quasi-geostrophic Rossby waves generated at the eastern boundary. The timescale for adjustment (the "setup time") depends on the time it takes for these waves to cross the basin, and so is a linear function of the zonal extent of the ocean. When equatorial Kelvin waves are present (as is usually the case) the adjustment does not proceed smoothly from east to west. Kelvin waves cause mass to oscillate back and forth across the basin so that the final state is not approached monotonically from the east and the adjustment time is lengthened.

Extra-equatorially ($|y| >> E$), the term $\gamma\,(\tilde{\mathbf{u}}-\tilde{\mathbf{u}})$ in (3.5a) is negligible for all time, but we know from the steady state solution discussed above that it must eventually become important in the equatorial vorticity balance. By rescaling (3.5) it may be shown that frictionally induced transport has a stream function π satisfying the time dependent version of (4.6); viz.

$$\left(\frac{\partial}{\partial t_*} + 1\right)\pi_{\zeta\zeta} + a\,\pi_x = -\,\tilde{\mathbf{u}}_\zeta^{(0)}\,.$$

As before, $\zeta=E^{-1}y$ while $t_*=\gamma t$ so that this component of the transport evolves on a timescale γ^{-1}: about 200 days for the values in Table 1. The height deviation associated with this transport remains small [$h=O(E)$].

5. Conclusion

The principal purpose of this paper has been the development of a simple model suitable for numerical experiments designed to give insight into the dynamics of the equatorial ocean circulation. There are two layers above the thermocline with *no density difference* between them. The ocean below the thermocline is modeled as a resting layer with a higher constant density. The surface layer is taken to be of constant depth while the depth of the lower active layer is dynamically determined. The two active layers exchange mass (and momentum, energy, etc.) via the vertical velocity at their interface. They are also frictionally coupled. This is the simplest vertical structure that allows a steady state undercurrent.

In our model the wind stress is taken up directly by the surface layer, which thus acts like an Ekman layer in a vertically continuous but homogeneous ocean. In a more realistic model—or the real ocean—it is the surface mixed layer that directly absorbs the wind stress and turbulently mixes the momentum input more or less uniformly throughout the depth of the layer.

Strictly, the wind stress enters the momentum equations as a boundary condition on the vertical shear. By integrating these equations in the vertical a layer model is obtained in which the stress appears as a body force driving the total momentum in the surface. As shown in Sec. 2 the conventional layered model (in which the layer below the surface has a different density and there is no mass exchange between layers) permits a steady state solution in which there is no motion for a curl-free wind stress. Such a model can miss the undercurrent when it should be present. More generally, these models will underestimate inertial effects because the effect of the wind stress is averaged over too great a depth. The mean velocity of the layer is much smaller than the velocity to be expected in the surface mixed (or Ekman) layer. (It is this turbulent surface layer that first becomes nonlinear.) For example, the calculation of O'Brien and Hurlbut (1974), while formally nonlinear, shows nearly linear behavior because the direct effect of the stress is not confined to a sufficiently shallow surface layer.

The linear steady state vertically integrated transport is given primarily by the Sverdrup (1947) balance. For spatially constant winds this Sverdrup transport vanishes. If the stress at the model thermocline is nonzero, there is additional vertically integrated transport in a frictional boundary layer centered on the equator. This layer thickens from east to west. The interior transports are predominantly zonal; a boundary current is required at the western side to close the fluid circuit. A zonal wind stress produces a net transport in the direction of the wind at the equator. This result shows that the *linear* model cannot produce vertically integrated

transport in the same direction as the observed (and model) undercurrent. The nonlinear dynamics must be included to get the correct result.

Two timescales for the evolution of the circulation are revealed by the analysis of the time dependent equations. The time for the boundary layer flow $\tilde{\mathbf{u}}$ to become established is $0(\gamma^{-\frac{1}{2}})$ — about 20 days for the parameters used in this model. The transports (or lower layer flow) cannot be establishel until the basin-wide pressure gradients are set up. This requires that mass be moved longitudinally across the basin, a task accomplished by equatorial Kelvin and Rossby waves. The setup time thus depends on the zonal extent of the ocean. It also depends on the nature of the forcing: the setup time is longer when Kelvin waves are a significant part of the ocean's response. In all cases the setup time will be at least 100 days for the present model.

Because (at least) the surface velocities in the vicinity of the equator quickly become large, it is clear that the flow becomes nonlinear. The nonlinear dynamics are investigated numerically in II. Those numerical experiments, together with similar experiments on the linear dynamics, will be interpreted in the light of the analytic results reported here.

Acknowledgments. I am grateful to my advisor, Professor J. G. Charney, for his guidance and encouragement. Several valuable conversations with Professor H. M. Stommel are gratefully acknowledged, as are helpful discussions with Professor Moshe Israeli concerning the model formulation. My special thanks to Dr. E. S. Sarachik, for providing invaluable criticisms throughout the course of this work. This work was supported by NASA Grant NGR 22-009-727 to the Massachusetts Institute of Technology.

REFERENCES

Blandford, R. 1966. Mixed Gravity-Rossby waves in the ocean. Deep Sea Res., *13,* 941–960.

Cane, M. A. 1975. A study of the wind-driven ocean circulation in an equatorial basin, Ph.D. Thesis, Masachusetts Institute of Technology, 372 pp.

—— 1978. The response of an equatorial ocean to simple wind stress patterns: II. Numerical results. J. Mar. Res., this issue.

Cane, M. M. and E. S. Sarachik. 1976. Forced baroclinic ocean motions: I. The linear equatorial unbounded case. J. Mar. Res., *34,* 629–665.

—— 1977. Forced baroclinic ocean motions: II. The linear bounded case. J. Mar. Res., *35,* 395–432.

Charney, J. G. 1955. The generation of ocean currents by wind. J. Mar. Res., *14,* 477–498.

—— 1960. Non-linear theory of a wind-driven homogeneous layer near the equator. Deep Sea Res., *6,* 303–310.

Charney, J. G. and S. Spiegel. 1971. Structure of wind driven equatorial currents in homogeneous oceans. J. Phys. Oceanogr., *1,* 149–160.

Düing, K., P. Hisard, E. Katz, J. Krauss, J. Meincke, K. Moroshkin, G. Philander, A. Rybnikov, and K. Voigt. 1975. Meanders and long waves in the Equatorial Atlantic. Nature, *257,* 280–284.

Fofonoff, N. P. and R. B. Montgomery. 1955. The equatorial undercurrent in the light of the vorticity equation. Tellus, *7,* 518–521.

Gill, A. E. 1971. The equatorial current in a homogeneous ocean. Deep Sea Res., *18,* 421–431.
—— 1975. Models of equatorial currents, *in* Proc. Symp. on Numerical Models of Ocean Circulation, Washington, D.C., Nat. Acad. Sci., 364 p.
Knauss, J. A. 1966. Further measurements and observations on the Cromwell Current. J. Mar. Res., *24,* 205–240.
Knox, R. A. 1976. On a long series of measurements of Indian Ocean equatorial currents near Addu Atoll. Deep Sea Res., *23,* 211–221.
Leetmaa, A. 1973. The response of the Somali Current at 2°S to the southwest monsoon of 1971. Deep Sea Res., *20,* 397–400.
Lighthill, M. J. 1969. Dynamic response of the Indian Ocean to onset of the southwest monsoon. Phil. Trans., Roy. Soc., *A 265,* 45–92.
Matsuno, T. 1966. Quasi geostrophic motions in the equatorial area. J. Met. Soc. Japan, *44,* 25–43.
McKee, W. D. 1973. The wind-driven equatorial circulation in a homogeneous ocean. Deep Sea Res., *20,* 889–899.
Munk, W. H. 1950. On the wind-driven ocean circulation. J. Meteorol., *7,* 79–93.
O'Brien, J. J. and H. E. Hurlbut. 1974. An equatorial jet in the Indian Ocean, Theory. Science, *184,* 1075–1077.
Pedlosky, J., 1968. An overlooked aspect of the wind-driven ocean circulation. J. Fluid Mech., *32,* 809–821.
Philander, S. G. H. 1971. The equatorial dynamics of a shallow homogeneous ocean. Geophys. Fluid Dyn., *2,* 219–245.
—— 1973a. The equatorial thermocline. Deep Sea Res., *20,* 69–86.
—— 1973b. Equatorial undercurrent: measurements and theories. Rev. Geophys., *11,* 513–570.
—— 1976. Instabilities of zonal equatorial currents. J. Geophys. Res., *81,* 3725–3735.
—— 1978. Forced oceanic waves. Rev. Geophys. Space Phys., *16,* 15–46.
Robinson, A. R. 1960. The general thermal circulation in the equatorial regions. Deep Sea Res., *6,* 311–317.
—— 1966. An investigation into the wind as the cause of the Equatorial Undercurrent. J. Mar. Res., *24,* 179–204.
—— 1970. Boundary layers in ocean circulation models in Annual Review of Fluid Mechanics *2,* Palo Alto, Annual Reviews Inc., 312 pp.
Stommel, H. 1948. The westward intensification of wind-driven currents. Trans. Amer. Geophys. Union, *29,* 202–206.
—— 1960. Wind-drift near the equator. Deep Sea Res., *6,* 298–302.
Sverdrup, H. D. 1947. Wind-driven currents in a baroclinic ocean, with applications to the equatorial currents of the eastern Pacific. Proc. Nat'l. Acad. Sci., *33,* 318–326.
Taft, B., B. Hickey, C. Wunsch and D. Baker. 1974. The Cromwell Current at 150°W. Deep Sea Res., *21,* 403–430.
Veronis, G. 1963a. On the approximations involved in transforming the equations of motion from a spherical to the β-Plane, part I. Barotropic systems, J. Mar. Res., *21,* 110–124.
—— 1963b. On the approximations involved in transforming the equations of motion from a spherical to the β-Plane, part II. Baroclinic systems, J. Mar. Res., *21,* 199–204.
Veronis, G. and H. Stommel. 1956. The action of variable wind stresses on a stratified ocean, J. Mar. Res., *15,* 43–75.
Williams, R. and C. Gibson. 1974. Direct measurement of turbulence in the Pacific Equatorial Undercurrent. J. Phys. Oceanogr., *4,* 104–108.

Received: *27 June, 1977;* revised: *22 November, 1978.*